Magnetic field effect on excited-state spectroscopies of π-conjugated polymer films

Bhoj R. Gautam, Tho D. Nguyen, Eitan Ehrenfreund, and Z. Valy Vardeny

Phys. Rev. B **85**, 205207 — Published 16 May 2012

DOI: 10.1103/PhysRevB.85.205207

Magnetic field effect on excited state spectroscopies of π-conjugated polymer films

Bhoj R. Gautam[1], Tho D. Nguyen[1], Eitan Ehrenfreund[1,2] and Z. Valy Vardeny[1]*

[1]*Departmentof Physics and Astronomy, University of Utah, Salt Lake City, UT 84112, USA*

[2]*Physics Department and Solid State Institute, Technion-Israel Institute of Technology, Haifa 32000, Israel*

Abstract

The magnetic field effect in organic light-emitting diodes, such as magneto-conductance and magneto-electroluminescence has been intensively explored in the last few years. Here we demonstrate magnetic field effect of two excited state *spectroscopies* in films of a prototype π-conjugated polymer, namely a soluble derivative of poly(phenylene-vinylene) [MEH-PPV]; these are magneto-photoinduced absorption (MPA) and magneto-photoluminescence (MPL). We study these novel magnetic field effects in pristine MEH-PPV films, MEH-PPV films subjected to prolonged illumination, and blend of MEH-PPV with a fullerene derivative. Being spectroscopic in nature, MPA and MPL are determined by the photoexcitation spin *density*, and thus may unravel the occurrence of a myriad of spin-mixing processes in organic semiconductors that include hyperfine interaction in polaron-pairs, spin-sublevel mixing in triplet excitons, triplet-triplet annihilation, and triplet-singlet collision. The recently observed ultra-small magnetic field effect at B<~0.5 mT in organic diodes is also observed in the MPA response of MEH-PPV films that support polaron photoexcitations, thereby identifying the underlying mechanism as due to spin-mixing of polaron-pairs by the hyperfine interaction.

* To whom correspondence should be addressed; e-mail: val@physics.utah.edu

I. Introduction

The intensive studies of magnetic field effect, such as magneto-conductance (MC) and magneto-electroluminescence (MEL) in organic light emitting diodes[1-12] was boosted in 2004, as the first prototype organic spin valve was demonstrated revealing the existence of relatively long spin coherence length in the organics[13]. Various possible mechanisms responsible for the MC and MEL in organic diodes have emerged from these studies. Some models have emphasized the influence of magnetic field on carrier mobility in the device[4, 8, 14, 15], while other models have emphasized the influence of the magnetic field on the carrier density, brought about by spin-dependent microscopic processes among polaron-pairs (PP) or triplet excitons (TE)[5, 12, 16]. A variety of spin-mixing mechanisms have been proposed that include the hyperfine interaction (HFI) between polarons and the skeleton protons in π-conjugated polymers and molecules[3, 4, 11, 12]; the difference, Δg in the electron and hole g-factors in polymer/fullerene blends[17-19]; a number of mechanisms that involve TE[5, 16]; and the spin-orbit coupling in small molecules that contain heavy atoms[3, 20]. Thus, the magnetic field effect in organic diodes has proven to be an especially rich and interesting research field.

Here we report a novel magnetic field effect of spectrally resolved photo-induced absorption (PA) and photoluminescence (PL) [dubbed hereafter MPA and MPL, respectively] in π-conjugated polymer *films* (as opposed to the previously studied organic diodes[21]), and apply it to study a number of spin-dependent processes. This 'spectroscopic-sensitive' magnetic field effect technique differs from the previously studied 'transport-related' MC and MEL in devices in two important respects. (i) Since PA and PL measure directly the density of the photoexcitations (such as PP and/or TE), then MPA and MPL can be directly related to the photoexcitation spin density. Consequently by directly comparing the MPA and MPL responses in films to those of MC and MEL in organic diodes based on the same organic active layer, we are able to relate the magnetic field effect in organic diodes to the spin *densities* of the excitations formed in the device. (ii) Being a spectroscopic technique, we can use the MPA as a new tool to discern various long-lived photoexcitations in organic semiconductor films. In addition we deduce the main spin-dependent species and/or spin-mixing mechanism that determine the MPA (MPL) response in three different forms of a well known π-conjugated polymer, including spin-mixing

in PP species, triplet-triplet annihilation, spin-mixing among the triplet spin sublevel, and Δg mechanism of PP in polymer/fullerene blends.

We studied MPA and MPL responses in a prototype π-conjugated polymer, namely MEH-PPV (see backbone structure in Figure 1(b)), which is a derivative of poly(phenylene vinylene) [PPV]. The three different forms that we studied are: pristine film; film exposed to prolonged UV illumination; and electron donor in MEH-PPV/PCBM blend having weight ratio 1:1. A schematic diagram of the philosophy underlying the MPA technique is presented in Figure 1(a). For obtaining PA the film is excited by a continuous wave (cw) laser beam with above-gap photon energy that generates steady state singlet excitons (SE; $S_0 \rightarrow S_1$). The SE may radiatively recombine ($S_1 \rightarrow S_0$); convert into long-lived TE via intersystem crossing; or separate into positive and negative charge polarons, some of which may form long-lived PP species. These various secondary reactions are symbolized by $S_1 \rightarrow X_0$, where X stands for species such as PP, TE and pairs of TE's. The X species has an excited state transition $X_0 \rightarrow X_1$ (PA_X), which is activated by a weak probe beam. PA is defined as the negative fractional change in transmission, T: $PA(E) \equiv (-\Delta T/T) = N_{SS}\beta(E)$, where N_{SS} is the species *steady state density*, β(E) is the photoexcitation optical cross-section, and E is the probe beam photon energy. Therefore in a magnetic field, B, $PA_X(B)$ is determined by the density $N_{SS}(B)$; which, in turn is proportional to the species generation rate G and the inverse of decay rate coefficient, $\kappa(B)$ [$N_{ss}=G/\kappa$, see also Section IV]. For $B \neq 0$ the X_0 level splits according to the relevant spin multiplicity, L (L=3, 4 and 9, respectively for the S=1 TE; PP composed of two S=½ polarons; and a pair of TE's). Consequently through specific spin-mixing processes, the spin content of each sub-level, its decay rate κ, and thus N_{SS} and consequently PA all become B-dependent that lead to the B dependent magneto-response $MPA_X(B) \equiv [PA_X(B)-PA_X(0)]/PA_X(0)$. In contrast since it originates from singlet exciton radiative recombination then MPL(B) cannot directly originate from SE (S=0, which is B-independent); but rather is caused indirectly, for example via SE collision with TE.

The paper is arranged as follows. The experimental technique is described in section II. In Section III we describe our experimental results on the three forms of MEH-PPV including comparative studies of films and devices. In pristine MEH-PPV films we assign the MPA as due to the TTA mechanism, while the MPL is assigned to TE-polaron scattering. In irradiated MEH-

PPV films we propose that the PP mechanism with hyperfine interaction mediated spin mixing is responsible for the obtained MPA. The same mechanism combined with another mechanism related to the different g-values of positive and negative polarons ('Δg mechanism') play a dominant role in the MPA response of MEH-PPV/PCBM blend film. In Section IV we describe an all-purpose quantum mechanical model which may explain the magnetic field effect obtained in all three MEH-PPV polymer forms. The model is based on the time evolution of the photogenerated species spin-sublevels in a magnetic field, in the presence of spin-dependent decay mechanism. This model is viable for MPA measurements in films as well as MC and MEL in devices made of the same polymers. Using this model we show that the magnetic field dependent excitation density may account for the measured magnetic effect in the MEH-PPV entire system that includes MPA, MPL, MC and MEL.

II. Experimental

For the MC and MEL measurements we fabricated ~5 mm^2 diodes, where the organic spacers were deposited on a hole transport layer: poly(3,4-ethylenedioxythiophene) [PEDOT]-poly(styrene sulphonate) [PSS]. We capped the bilayer structure with a transparent anode: indium tin oxide [ITO], and a cathode: calcium (protected by aluminum film). The devices were driven at constant bias, V. For the PL and PA measurements we used a standard photomodulation set-up [22]. For excitation we used a cw Ar^+ laser pump beam at $\hbar\omega_L$=2.54 eV that was modulated at frequency f; and an incandescent tungsten/halogen lamp as the probe. The PA signal, $\Delta T/T$ is the fractional change, ΔT in transmission, T, which is negative for PA and positive for photobleaching (PB). The PA signal was measured using a lock-in amplifier referenced at f, a monochromator, and various combinations of gratings, filters, and solid-state photodetectors spanning the spectral range $0.3<\hbar\omega$(probe)<2.3 eV. This setup was also used for measuring the PL spectrum[22]. The device (or film) was placed in a cryostat in between the two poles of an external magnetic field up to 300 mT. For obtaining the desired magnetic field response, the measured quantity such as PA and PL in films, and EL and current in diodes were measured while sweeping B.

MEH-PPV films are somewhat unusual in the class of π-conjugated polymers since their PA spectrum may change according to the environment/mixture used, as previously shown in detail[22]. Films of pristine MEH-PPV that are kept in the dark for a long time show fairly strong PL emission (quantum efficiency of about 25%), and their PA spectrum consists of long-lived triplet excitons, namely PA_T (Figure 2a); but do not support long-lived photogenerated polarons because of small density of imperfections and impurities in the film. However if the same films are exposed to prolonged UV illumination a meta-stable state is formed due to photoinduced native defects in the film, in which the PA spectrum also contains substantial long-lived photogenerated polarons having two characteristic PA bands (PA_P) that are formed on the expense of both PL and PA_T[22]. The process is reversible when subjected to elevated temperatures in the dark. Furthermore when the MEH-PPV donor-like polymer is mixed with a fullerene acceptor-like molecule that form bulk heterojunction morphology, then the photogenerated excitons ionize to form positive polarons on the polymer and negative polarons on the fullerene molecule [23]. We took advantage of these MEH-PPV film properties to obtain MPA of various photoexcitation species using the same polymer film; namely before and after prolonged UV illumination, and in blend with fullerene molecules, namely [6,6]-phenyl-C_{61}-butyric acid methyl ester (PCBM).

III. Experimental results and interpretation

A. Pristine MEH-PPV films

In Figure 2(a) we show the PA spectra of pristine MEH-PPV film at B=0 and 100 mT, respectively. The spectrum consists of a broad PA band centered at ~1.37 eV (marked T) that is assigned to TE transition (PA_T)[22]; no other PA bands were obtained down to 0.2 eV that attests of the good quality of the polymer used here. The B=100 mT spectrum is identical in shape to that of B=0, except that is slightly weaker. The difference, ΔPA spectrum is similar to PA_T demonstrating that it relates to the TE steady state density. As seen in Figure 2(b) the magnetic field response, $MPA_T(B) \equiv \Delta PA/PA_T$ varies strongly with the laser excitation intensity, I_L, and thus with N_{SS} (which is proportional to I_L). N_{SS} is also inversely proportional to the sub-level TE

effective recombination rate constant, $\kappa=\sum\kappa_\alpha$ *(α=1,..,L)*, which are *B*-dependent. At small I_L $MPA_T(B)$ monotonically decreases, but it gradually transforms into a more complex response at large I_L where two components are resolved; a low-field MPA component that decreases with *B*, and a high-field component that increases with *B*. We thus conclude that $MPA_T(B)$ is dominated by two different spin-mixing mechanisms related with TE species; one mechanism that dominates at low I_L which may be a 'single-TE' process; and the other mechanism that increases at large I_L, and therefore most likely involves 'triplet-triplet annihilation' (TTA) process.

The same pristine MEH-PPV film also shows MPL response. Figure 2(a) inset displays the PL spectrum at *B*=0 and 100 mT, respectively that consists of several vibronic replicas, with 0-0 transition at 2.05 eV. The difference, ΔPL spectrum follows the PL spectrum, and is thus assigned to the $S_1 \rightarrow S_0$ transition (Figure 1(a)). Unlike $MPA_T(B)$, however Figure 2(c) shows that MPL(*B*) does not change with I_L; it monotonically decreases with *B*, similar to the low intensity $MPA_T(B)$, i.e. the low-field magnetic field component. Since singlet excitons alone cannot depend on the magnetic field, we therefore assign this MPL(*B*) response as due to SE *non-radiative decay* that is activated by 'collisions' with TE species, of which density $N_{SS}(B)$ also determines the $MPA_T(B)$ response at low I_L.

B. Irradiated MEH-PPV films and devices

Entirely different characteristic PA and MPA properties were measured in the same MEH-PPV film after prolonged UV irradiation (~150 minutes at 50 K using a Xenon lamp), which supports photogenerated polaron species[22]. Figure 3(a) shows the PA spectrum of irradiated MEH-PPV film at *B*=0 and 100 mT, respectively at similar excitation intensities as used above for the pristine film. The spectrum in this case consists of two broad PA bands; one centered at ~0.4 eV that is assigned to the lower polaron transition (marked 'P_1'); and the other is asymmetric with a peak at ~1.4 eV (marked '$T+P_2$') that is composed of the polaron P_2 transition centered at ~1.55 eV, and the remnant of the TE transition, PA_T[22]. The spectrally resolved difference *ΔPA* (Figure 3(a)) shows that MPA in this MEH-PPV form is correlated only with the two polaron PA bands P_1 and P_2, but not with that of PA_T. This is one of the MPA technique advantages; *its ability to spectrally resolve the dominant species and spin-dependent process*. We assign *ΔPA* spectrum here to magnetic field dependence of the PP's density, namely ΔPA_{PP}. Unlike the negative ΔPA_T

of the pristine sample Figure 2(a)) we found $\Delta PA_{PP}>0$ in the irradiated sample, which suggests that a different spin-mixing mechanism is dominant in the present case. The positive monotonically increasing $MPA_{PP}(B)$ (Figure 3(b)) is naturally explained by the PP mechanism, in which the spin-mixing is governed by the HFI[12] (see below).

For comparison we also show MC(B) and MEL(B) (Figure 3(c)) obtained in MEH-PPV diodes. The MC and MEL responses are identical to each other; and, in addition *are very similar to the* $MPA_{PP}(B)$ response shown in Figure 3(b). This indicates that all three magnetic field effects share a common origin. Since MPA(B) does not involve carrier transport, we thus conclude that MC(B) and MEL(B) obtained in the devices *need not involve transport*. All three responses can be explained equally well by the microscopic PP model presented below, which involves magnetic field dependence of the species' spin sublevel character and their *density*, rather than transport-related mechanism within the organic interlayer of the device.

A salient feature of the low field (B<1.2 mT) $MPA_{PP}(B)$ response is shown in Figure 3(e). Interestingly this response (dubbed here ultra-small MPA, or USMPA) was measured at 1.1 eV probe photon energy, where the PA spectrum actually shows photo-bleaching (PB, Figure 3(a)). The 1.1 eV MPA is shown on a larger B-scale in Figure 3(e) inset; it has in fact the same response as MPA at 1.4 eV. With increasing |B| the USMPA response decreases for $|B|$<0.6 mT before increasing again to form the monotonic response seen at larger fields. Similar non-monotonic response was previously observed in both MC(B) and MEL(B) in organic diodes[12, 24], and was explained as due to level-crossing at B=0 that involves spin sublevels formed by the polaron-proton HFI in the polymer chains. Therefore the same explanation is viable also for the USMPA component here. We note that the USMPA is not related to transport in an organic device; in addition it occurs at field values close to the *earth magnetic field* (≈0.05 mT). We thus infer that the USMPA in polymers (and other organic molecules[11]) could, in principle be used by a variety of living creatures on earth that may take advantage of the earth magnetic field to augment their activity; such as navigation for example, as shown previously[25].

C. Films and devices of MEH-PPV/PCBM blends

Yet a third type of MPA response is viable in films of MEH-PPV/PCBM blend. Upon laser excitation of the polymer (PCBM does not absorb in the visible spectral range), the singlet excitons quickly dissociate into hole-polarons on the MEH-PPV chains and electron-polarons on the PCBM molecules [23]. This weakens the PL intensity of the MEH-PPV chains, and completely eliminate the triplet PA_T band from the PA spectrum[26]. Therefore the PA spectrum in this case (Figure 4(a)) consists of PA of positive polarons on the MEH-PPV chains (P_1 at ~0.4 eV, and P_2 at ~1.37 eV, respectively), as well as PA band of negative polarons on the PCBM (C_{61}^- at ~1.2 eV). Importantly the positive and negative polarons have different gyro-magnetic g-values[27], with $\Delta g \equiv [g(\text{MEH-PPV}) - g(\text{PCBM})] \approx 3 \times 10^{-3}$. This occurs since the P^+ and P^- species are separated in the blend onto two different environments (polymer and fullerene matrices, respectively).

ΔPA spectrum in the blend (Figure 4(a)) is negative, and is assigned to PP transition of both positive and negative polarons. $MPA_{PP}(B)$ response in this case (Figure 4(b)) has two components: a low-field component that sharply decreases with B, followed by a high-field component that slowly increases with B forming an apparent minimum at B<~10 mT. For comparison we also show MC(B) response (Figure 4(c)) of a photovoltaic device based on the same blend, where again two MC(B) components are visible[9]; except that the MC response is opposite in sign compared to that of MPA. The stunning similarity obtained between $MPA_{PP}(B)$ and MC(B) shows that they share the same underlying mechanism. Owing to the finite Δg of the positive and negative polarons in the blend, both $MPA_{PP}(B)$ and MC(B) (Figure 4(c)) can be accounted for by the PP model that includes the HFI (low-field component) and Δg mechanism (high-field component[9]) as explained below in Section IV. Importantly similar to the irradiated MEH-PPV films (Figure 3(e)), a modulated MPA response near B~0 is also seen in the blend as shown in Figure 4(b) inset; but it occurs at much lower fields, i.e. B<0.1 mT.

IV. Discussion in terms of an all-purpose quantum mechanical model

In the following we introduce a general model for explaining the magnetic field responses in all three forms of MEH-PPV films. In our previous publications[11, 12, 24, 28] we showed that using a relatively simple model spin-Hamiltonian that includes PP spins subjected to HFI in a magnetic field, all of the important features of MC(B) and MEL(B) responses in organic diodes could be

explained. Here we generalize the model to include the 'Δg mechanism', as well as the effects of TE and TTA on MPA(B) and MPL(B) responses.

We consider a system that includes N identical species each with spin S having overall multiplicity L. For a system with a pair of polarons: N=2, S=½ and L=$(2S+1)^N$=4; for a single TE: N=1, S=1 and L=3; and for a pair of TE's: N=2, S=1, and L=9. According to the angular momentum addition rules the combined pair system is composed of spin multiplets having spin J=2S, 2S-1,..,0. Therefore the PP system is composed of triplet and singlet; whereas the pair of TE's is composed of quintet, triplet and singlet. When the HFI is taken into account and assuming that each species i interacts with N_i nuclei, each with spin I_{ji} $(j=1,..,N_i)$, then the total configuration space is of dimension $M=\Pi_{i=1}^{N}(2S_i+1)\Pi_{j=1}^{N_i}(2I_{ji}+1)$, where S_i=S is the species spin. For example for a PP system where each polaron of S=½ interacts with a single proton I=½, we obtain M=16.

Realizing the unique role of species decay in all magnetic field measurements[16, 29, 30], we describe the system by a spin Hamiltonian that includes a non-Hermitian relaxation term[29, 31], H_R

$$H = H_Z + H_{HF} + H_R \ , \tag{1}$$

where H_R describes the decay pathways of the spin multiplets:

$$H_R = -i\frac{\hbar}{2}\sum_{\alpha=1}^{L}\kappa_\alpha P^\alpha \ , \tag{2}$$

In Eq. (2) P^α ($\sum P^\alpha = \tilde{1}$) and κ_α are the relevant spin projection operators and decay rates, respectively. We emphasize that a finite magnetic field response can be obtained only when κ_α are spin dependent (see Eq. (5) below). In Eq. (1) the Zeeman term is: $H_Z = \mu_B \sum_{n=1}^{N} g_n \vec{S}_n \cdot \vec{B}$, where the summation is over all species assuming isotropic g-factor; and the HFI term is: $H_{HF} = \sum_{i=1}^{N}\sum_{j=1}^{Ni}[S_i \cdot \tilde{A}_{ij} \cdot I_{ji}]$. We assume for simplicity an isotropic HFI, and we also ignore the exchange interaction[12]. The time evolution of the density operator is now expressed as[31],

$$\sigma(t) = \exp(-iHt/\hbar)\sigma(0)\exp(iH^{\dagger}t/\hbar)\ , \tag{3}$$

where $H^{\dagger}$ is the Hermitian conjugate of H (note that $H^{\dagger} \neq H$), and the t=0 density matrix $\sigma(0)$ is determined by the generation process. The time dependent probability for the system in the α^{th} spin state may now be written as:

$$\rho_{\alpha}(t) = Tr(P^{\alpha}\sigma(t)) = \frac{L}{M}\sum_{n,m=1}^{M} P^{\alpha}_{n,m}\sigma_{m,n}(0)\cos(\omega_{mn}t)\exp(-\gamma_{mn}t)\ , \tag{4}$$

where $E_n = \hbar(\omega_n - i\gamma_n)$ (here n=1,…M; and ω_n, γ_n are real quantities) are the complex eigen-values of the non-Hermitian H, and $\omega_{nm} = \omega_n - \omega_m$; $\gamma_{nm} = \gamma_n + \gamma_m$. We emphasize that when the decay rates κ_{α} are spin dependent, γ_{nm} in Eq. (4) are not uniform and the decay of $\rho_{\alpha}(t)$ becomes spin dependent; this assures a finite magnetic field effect. The measured field response (e.g. MPA(B), MC(B), etc.) may be readily calculated using Eq. (4). In any of these processes the X species undergoes a specific reaction; e.g. $X_0 \rightarrow X_1$ (Figure 1(a)) for MPA, or dissociation into free polarons in the case of MC. Let R_{α} be the reaction rate constant, then the total yield of the reaction is:

$$\Phi_X = \sum_{\alpha=1}^{L}\int_0^{\infty} R_{\alpha}\rho_{\alpha}(t)dt = \frac{L}{M}\sum_{\alpha=1}^{L} R_{\alpha}\sum_{n,m=1}^{M} P^{\alpha}_{nm}\sigma_{mn}(0)\frac{\gamma_{nm}}{\gamma_{nm}^2 + \omega_{nm}^2}\ . \tag{5}$$

Equation (5) is a general expression from which any of the magnetic field effects considered here may be calculated via:

$$MX(B) = \frac{\Phi_X(B) - \Phi_X(0)}{\Phi_X(0)}, \tag{6}$$

In Eq. (6) X designates the magnetic field effect: X=PA, PL, C or EL for MPA, MPL, MC or MEL, respectively. For example in the case of PA when assuming that the optical cross section is spin independent, $R_{\alpha} \equiv R$ in Eq. (5), and $\Phi_{PA} = R\sum_{\alpha}\int \rho_{\alpha}(t)dt = (2RL/M)\sum_n \sigma_{nn}(0)/\gamma_n \propto N_{SS}$. Consequently MPA$(B)=[N_{SS}(B)-N_{SS}(0)]/N_{SS}(0)$, i.e. the MPA response is determined by the magnetic field dependent steady state polaron (or TE) population. These populations become magnetic field dependent due to the spin dependent decay rates κ_{α}. Likewise in the case of MC

the reaction rates R_α designate the spin dependent dissociation rate coefficient d_α, and the dissociation yield Φ_d is given by Eq. (5) where R_α is replaced by d_α. In each case the species involved as well as the recombination and intersystem crossing pathways are different, thus producing a unique response.

In the following we discuss five different magnetic field processes, and compare the model with the obtained experimental results.

(a) **MPA due to TE mechanism**. In pristine MEH-PPV films at low I_L (Figure 2(b) for I_L=10 mW), the photogenerated TE density is low, and this leads to very low density of TE pairs. Consequently the TE density in this case is determined by a recombination process in which the spin sub-level recombination constants κ_α (α=±1,0) are different from each other. The principal TE zero-field splitting (ZFS) parameters were obtained in MEH-PPV by the PA detected magnetic resonance technique; they are $D/g\mu_B \approx 63$ mT and $E/g\mu_B \approx 9$mT[32]. Using these ZFS parameters we calculated the energy levels and wavefunctions of a TE in a magnetic field applied in a general direction. Ignoring the relatively small HFI, we further calculated the powder pattern of $MPA_T(B)$ as shown in Figure 2(d) (TE) for $\kappa_1=\kappa_{-1}=0.25\kappa_0=1.3\times10^7 s^{-1}$. We note that: (a) this model also explains MPL(*B*) because TE-SE scattering that controls the exciton PL intensity (Figure 1(a)) is directly proportional to the TE density; and (b) this mechanism is unique in that it involves just one type of photoexcitation (as opposed to PP or pair of TE), and has not been considered before. The spin selectivity here arises from the spin dependent decay constants κ_α.

(b) **MPA due to TTA mechanism**. When pristine MEH-PPV films are subjected to high laser excitation intensity (Figure 2(b) for I_L=400 mW), then the TE density is sufficiently high that the TTA process becomes dominant. Consequently the triplet steady state density, N_{SS} is determined by the individual decay rates of the TE-TE collision byproducts, namely quintet, triplet and singlet states[16]. First we calculated the energy levels and wavefunctions of a pair of randomly oriented TE's in a magnetic field of a general direction. Subsequently using Eq. (5) and neglecting the relatively small HFI, the powder pattern response $MPA_{TTA}(B)$ was calculated as shown in Figure 2(d) (TTA) for $\kappa_Q=\kappa_T=\kappa_S/30=10^6 s^{-1}$.

(c) **MPA due to PP mechanism**. In UV irradiated MEH-PPV films the PA is dominated by polarons, and thus MPA originates from photogenerated PP species (Figure 3(b)). The calculated $MPA_{PP}(B)$ response using the PP mechanism is governed by the HFI as shown in Figure 3(d) [for the simulations shown in Figures 3 and 4 we assumed for simplicity that each polaron interacts with a single protons of spin I = ½; similar results were obtained for a larger number of protons]. For the calculation we used PP(triplet) to PP(singlet) recombination ratio, $\kappa_T/\kappa_S=0.96$ and isotropic HFI $a/g\mu_B$=3mT.

In the MEH-PPV/PCBM blend, the photoexcited positive and negative polarons have different g-factors[27]. Using the same parameters as above, and $\Delta g=3x10^{-3}$ (Ref [27]) we calculated the $MPA_{PP}(B)$ response as shown in Figure 4(d).

(d) **USMPA.** Some of the photoinduced PP dissociate to free polarons; thus the free polaron density becomes *B*-dependent that leads to free-polaron PA(*B*). As was shown previously[12] (and can also be calculated directly from Eq. (5)), the dissociated polaron density shows ultra-small magnetic field effect in agreement with Figure 3(e).

(e) **MC.** In Figure 4(e) we show MC(*B*) response calculated using Eq. (5) (assuming PP dissociation into free polarons) with: (i) HFI: $a/g\mu_B$=3mT and $\Delta g=0$, and (ii) same HFI with varying Δg, for the same parameters as in (c) above.

In all of these cases the agreement between the experimental data and calculated responses is a strong indication that the models used capture the main features of the experimental findings. Our model is very general, and may be applicable also when the exchange interaction, spin orbit coupling and a diffusion process are included. Our work shows that all specific forms of the organic magnetic field effect are based on the *same principles*, namely magnetic field manipulation of the spin density of the excited species, regardless whether they are formed via photon absorption (MPA and MPL in films) or carrier injection (MC and MEL in devices).

V. Summary

We have introduced a novel 'spectroscopic-sensitive' magnetic field effect technique which spectrally resolve photo-induced absorption and photoluminescence in π-conjugated polymer

films, and apply it to study a number of spin-dependent processes. By directly comparing the new MPA and MPL responses in films to those of MC and MEL in organic diodes based of the same organic active layer, we are able to relate the magnetic field effect in organic diodes to the spin *densities* of the excitations formed in the active layer of the device, regardless whether they are formed by photon absorption or carrier injection from the electrodes. We deduced the main spin-dependent species and/or spin-mixing mechanism that determine the MPA (MPL) response in three different forms of a π-conjugated polymer, namely MEH-PPV. These include spin-mixing in PP species, triplet-triplet annihilation, spin-mixing among the triplet spin sublevel, and Δg mechanism of PP in polymer/fullerene blends. We have introduced an all-purpose quantum mechanical model which is able to explain the obtained magnetic field response in the MEH-PPV system. This model is viable for both MPA response obtained in films as well as for MC and MEL responses obtained in devices made of the same organic interlayer as in the films. When we apply this model to the obtained results, we show that the magnetic field dependent excitation density may account for *all field responses* measured in the MEH-PPV system that include MPA, MPL, MC and MEL.

Acknowledgements

This work was supported in part by the NSF (Grant No. DMR-1104495 and MRSEC program at the UoU, grant No. DMR 1121252); the Israel Science Foundation (ISF 472/11; E.E.), and the US-Israel BSF (Grant # 2010135 ; Z.V.V. and E.E.).

References

1. O. Mermer, G. Veeraraghavan, T. L. Francis, Y. Sheng, D. T. Nguyen, M. Wohlgenannt, A. Kohler, M. K. Al-Suti and M. S. Khan, Phys. Rev. B **72**, 205202 (2005).
2. Y. Iwasaki, T. Osasa, M. Asahi, M. Matsumura, Y. Sakaguchi and T. Suzuki, Phys. Rev. B **74**, 195209 (2006).
3. V. Prigodin, J. Bergeson, D. Lincoln and A. J. Epstein, Synthetic Met **156**, 757-761 (2006).
4. P. A. Bobbert, T. D. Nguyen, F. W. A. v. Oost, B. Koopmans and M. Wohlgenannt, Phys. Rev. Letters **99**, 216801 (2007).
5. P. Desai, P. Shakya, T. Kreouzis, W. P. Gillin, N. A. Morley and M. R. J. Gibbs, Phys Rev B **75**, 094423 (2007).
6. B. Hu and Y. Wu, Nat Mater **6**, 985-991 (2007).
7. Y. Wu, Z. Xu, B. Hu and J. Howe, Phys. Rev. B **75**, 035214 (2007).
8. J. D. Bergeson, V. N. Prigodin, D. M. Lincoln and A. J. Epstein, Phys. Rev. Letters **100**, 067201 (2008).
9. F. J. Wang, H. Bässler and Z. V. Vardeny, Phys. Rev. Letters **101**, 236805 (2008).
10. S. Majumdar, H. S. Majumdar, H. Aarnio and R. Osterbacka, Phys. Status Solidi RRL **3**, 242-244 (2009).
11. T. D. Nguyen, B. R. Gautam, E. Ehrenfreund and Z. V. Vardeny, Phys Rev Lett **105** (2010).
12. T. D. Nguyen, G. Hukic-Markosian, F. J. Wang, L. Wojcik, X. G. Li, E. Ehrenfreund and Z. V. Vardeny, Nat Mater **9**, 345-352 (2010).
13. Z. H. Xiong, D. Wu, Z. V. Vardeny and J. Shi, Nature **427**, 821-824 (2004).
14. B. Hu, L. Yan and M. Shao, Adv Mater **21**, 1500–1516 (2009).
15. F. Wang, J. Rybicki, K. A. Hutchinson and M. Wohlgenannt, Phys Rev B **83**, 241202 (2011).
16. R. E. Merrifield, Pure and Applied Chemistry **27**, 481-498 (1971).
17. U. E. Steiner and T. Ulrich, Chem. Rev. **89**, 51-147 (1989).
18. H. Hayashi, *Introduction to dynamic spin chemistry; magnetic field effects on chemical and biochemical reactions*. (World Scientific Publishing Co., Singapore, 2004).
19. F. J. Wang, H. Bassler and Z. V. Vardeny, Phys. Rev. Letters **101**, 236805 (2008).
20. J. Rybicki, T. D. Nguyen, Y. Sheng and M. Wohlgenannt, Synthetic Met **160**, 280-284 (2010).
21. T. D. Nguyen, J. Rybicki, Y. Sheng and M. Wohlgenannt, Phys. Rev. B **77**, 035210 (2008).
22. T. Drori, E. Gershman, C. X. Sheng, Y. Eichen, Z. V. Vardeny and E. Ehrenfreund, Phys. Rev. B **76**, 033203 (2007).
23. N. S. Sariciftci, L. Smilowitz, A. J. Heeger and F. Wudl, Science **258**, 1474-1476 (1992).
24. T. D. Nguyen, B. R. Gautam, E. Ehrenfreund and Z. V. Vardeny, Synthetic Met **161**, 604-607 (2011).
25. K. Maeda, K. B. Henbest, F. Cintolesi, I. Kuprov, C. T. Rodgers, P. A. Liddell, D. Gust, C. R. Timmel and P. J. Hore, Nature **453**, 387-391 (2008).
26. X. Wei, Z. V. Vardeny, N. S. Sariciftci and A. J. Heeger, Phys Rev B **53**, 2187 (1996).
27. A. Konkin, U. Ritter, P. Scharff, H. K. Roth, A. Aganov, N. S. Sariciftci and D. A. M. Egbe, Synthetic Met **160**, 485-489 (2010).

28. T. D. Nguyen, G. Hukic-Markosian, F. Wang, X.-G. Li, E. Ehrenfreund and Z. V. Vardeny, Synthetic Met **161**, 598-603 (2011).
29. C. R. Timmel, U. Till, B. Brocklehurst, K. A. McLauchlan and P. J. Hore, Mol Phys **95**, 71-89 (1998).
30. J. Kalinowski, M. Cocchi, D. Virgili, P. Di Marco and V. Fattori, Chem Phys Lett **380**, 710-715 (2003).
31. J. Tang and J. R. Norris, Chem Phys Lett **92**, 136-140 (1982).
32. X. Wei, B. C. Hess, Z. V. Vardeny and F. Wudl, Phys Rev Lett **68**, 666 (1992).

Figure captions

FIG. 1. (color on line) Schematic illustration of the magnetic field dependent pump-probe PA processes. (a) The pump beam with above gap photon energy $h\nu_L$ excites the polymer MEH-PPV to the singlet exciton (SE) level ($S_0 \rightarrow S_1$). The SE relaxes via intersystem crossing to a triplet exciton (TE) or ionizes into separate charges forming polaron pair, PP ($S_1 \rightarrow X_0$). The steady state density of the X species is controlled by the spin dependent decay coefficient, κ. The incandescent probe beam monitors the photoinduced absorption, PA ($X_0 \rightarrow X_1$, PA_X), which is proportional to the X_0 steady state density. In a magnetic field $B>0$, X_0 splits according to its spin multiplicity, and the decay rate of each spin sub-level becomes field dependent, resulting in a B-dependent density and PA_X (thus forming MPA_X). (b) The backbone structures of MEH-PPV [2-methoxy-5-(2'-ethylhexyloxy)-poly(p-phenylene vinylene) [PPV] polymer, and the fullerene PCBM [phenyl-C_{61}-butyric acid methyl ester] molecule.

FIG 2. (color on line) Excited state spectra (PA and PL) and magnetic field effects in pristine MEH-PPV films. (a) The triplet PA band, PA_T at B=0 and 100 mT (black and red lines, respectively), generated using a laser excitation at $h\nu_L$=2.54 eV @ I_L=200 mW/cm^2, and their difference spectrum $\Delta PA_T=[PA_T(100mT)-PA_T(0)]$ (blue line). The region near the peak is magnified (within a circle). Right inset: PL spectrum at B=0 (black line) and 100 mT (red line). The lines in the circles show the data on a higher resolution scale. (b) $MPA_T(B)$ response measured at 1.37 eV probe, for various laser excitation intensities (normalized). (c) MPL(B) response measured at 2.05 eV probe for various laser excitation intensities (normalized). (d) Model calculations of $MPA_T(B)$ response using the TE mechanism (blue line, corresponds to the 10 mW data in (b)) and TTA mechanism (green line, corresponds to the 400 mW data in (b)); see text. (e) Model calculation of MPL(B) response using the model of singlet exciton quenching by TE (SE-TE collision, see text Section IV).

FIG. 3. (color on line) Excited state spectra and magnetic field effects in UV irradiated MEH-PPV film and in organic light emitting diode. (a) PA spectrum at I_L=100 mW/cm^2 for B=0 (black line) and B=100 mT (red line) and their difference spectrum, $\Delta PA=[PA(100mT)-PA(0)]$ (blue line) in MEH-PPV film. (b) MPA(B) response measured at 1.4 eV probe for various laser excitation intensities (normalized). (c) MEL(B) and MC(B) responses in MEH-PPV diode. (d) Model calculations of $MPA_{PP}(B)$ response in MEH films using the PP mechanism (see text). (e) MPA(B) response at 1.1 eV probe up to B=1.5 mT (filled squares) and B=60 mT (blue line, inset).

FIG. 4. (color on line) Excited state spectra and magnetic field effects in MEH-PPV/PCBM film and diode. (a) PA spectrum of MEH-PPV film at I_L=mW/cm^2 for B=0 (black line) and B=15 mT (red line), respectively, and their difference spectrum, $\Delta PA=PA(15mT)-PA(0)$ (blue line). (b) MPA(B) response measured at 1.37 eV probe for various laser excitation intensities (normalized). Inset: high resolution data, showing USMPA peaks at |B|~0.1 mT. This data was measured upon shielding from the earth magnetic field and any stray field. (c) MC(B) response in a diode at various bias voltages, V. (d) and (e) Model calculations of $MPA_{PP}(B)$ and MC(B) response, respectively, using the 'Δg + HFI' mechanism (see text, Section IV).

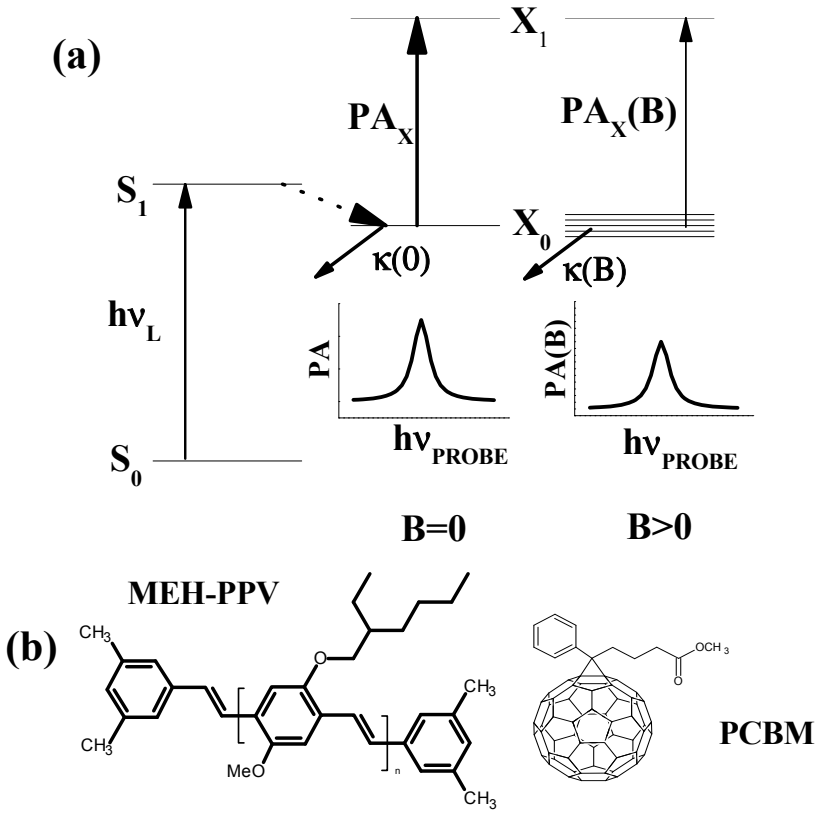
(a)
X1
PAX
PAX(B)
S1
X0
κ(0)
κ(B)
hνL
PA
PA(B)
hνPROBE
hνPROBE
S0
B=0
B>0
(b)
MEH-PPV
CH3
CH3
O
CH3
MeO
n
CH3
OCH3
O
PCBM

Figure 1

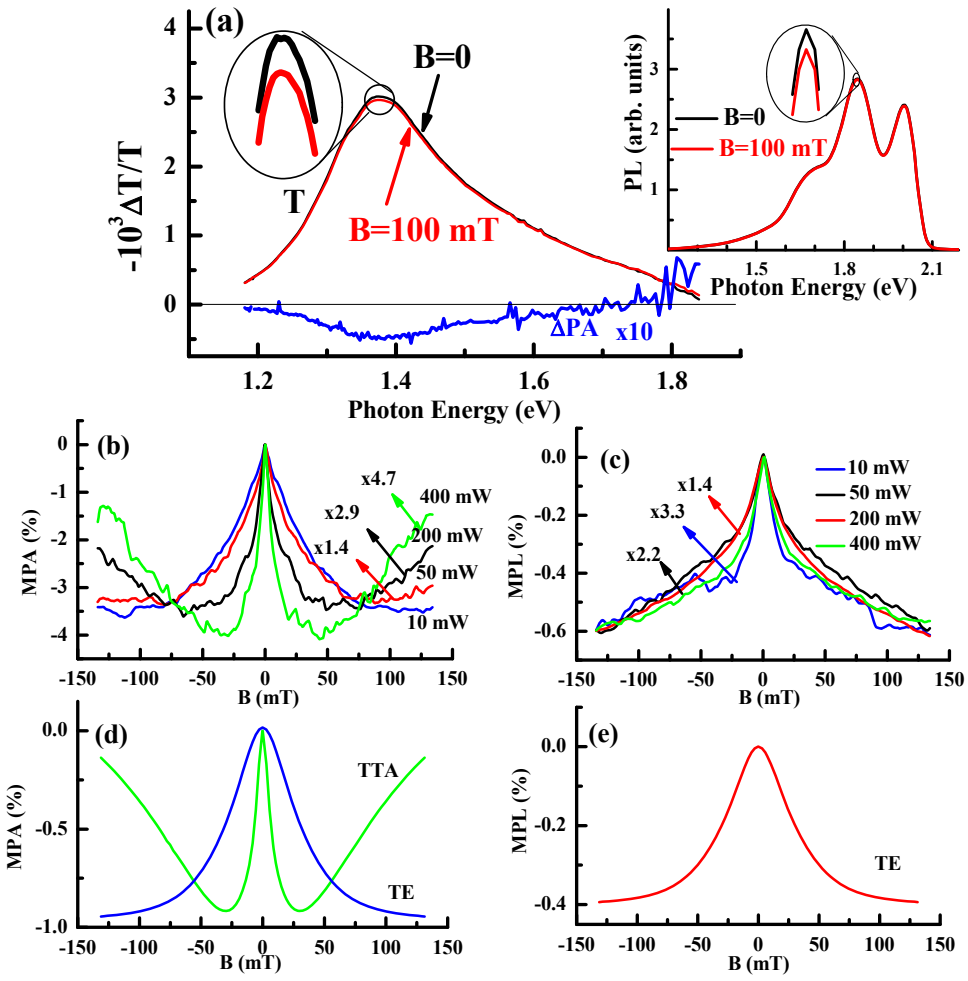
(a)
B=0
B=100 mT
T
-10^3ΔT/T
ΔPA x10
Photon Energy (eV)
PL (arb. units)
B=0
B=100 mT
Photon Energy (eV)
(b)
MPA (%)
x4.7
x2.9
x1.4
400 mW
200 mW
50 mW
10 mW
B (mT)
(c)
MPL (%)
x1.4
x3.3
x2.2
10 mW
50 mW
200 mW
400 mW
B (mT)
(d)
MPA (%)
TTA
TE
B (mT)
(e)
MPL (%)
TE
B (mT)

Figure 2

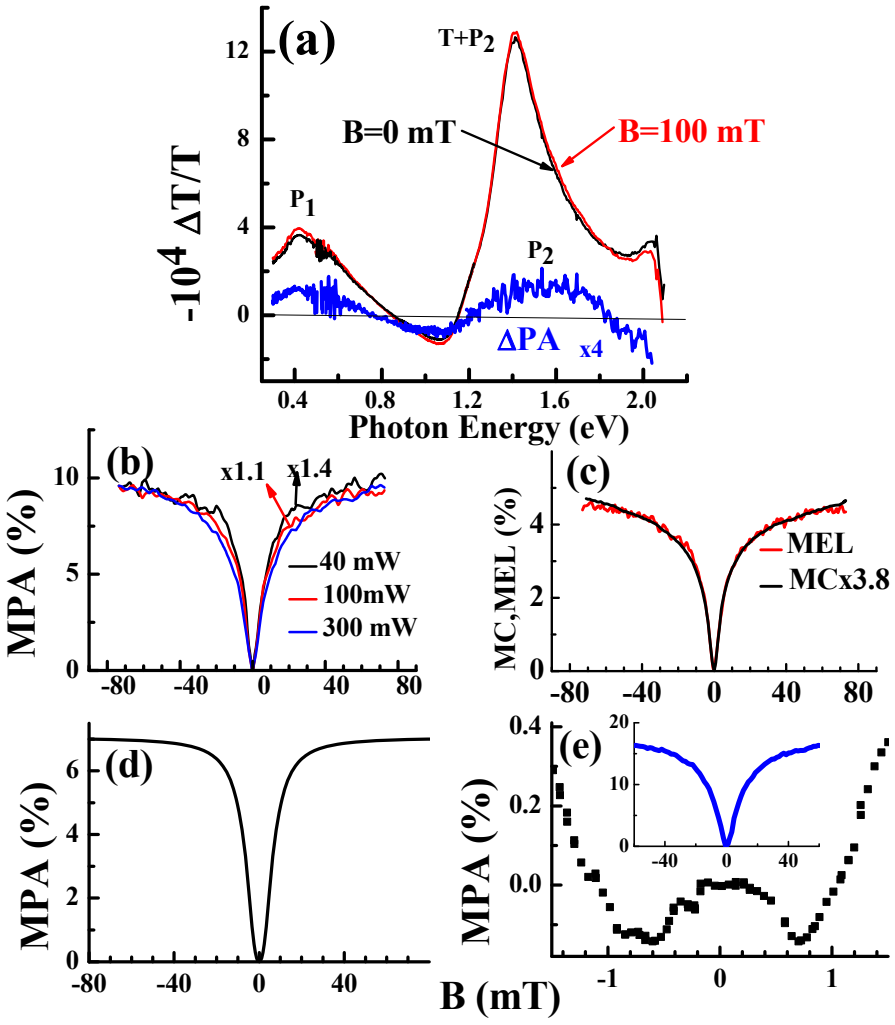
(a)
T+P2
B=0 mT
B=100 mT
P1
P2
ΔPA x4
-10^4 ΔT/T
Photon Energy (eV)
(b)
x1.1
x1.4
40 mW
100mW
300 mW
MPA (%)
(c)
MEL
MCx3.8
MC,MEL (%)
(d)
MPA (%)
(e)
MPA (%)
B (mT)

Figure 3

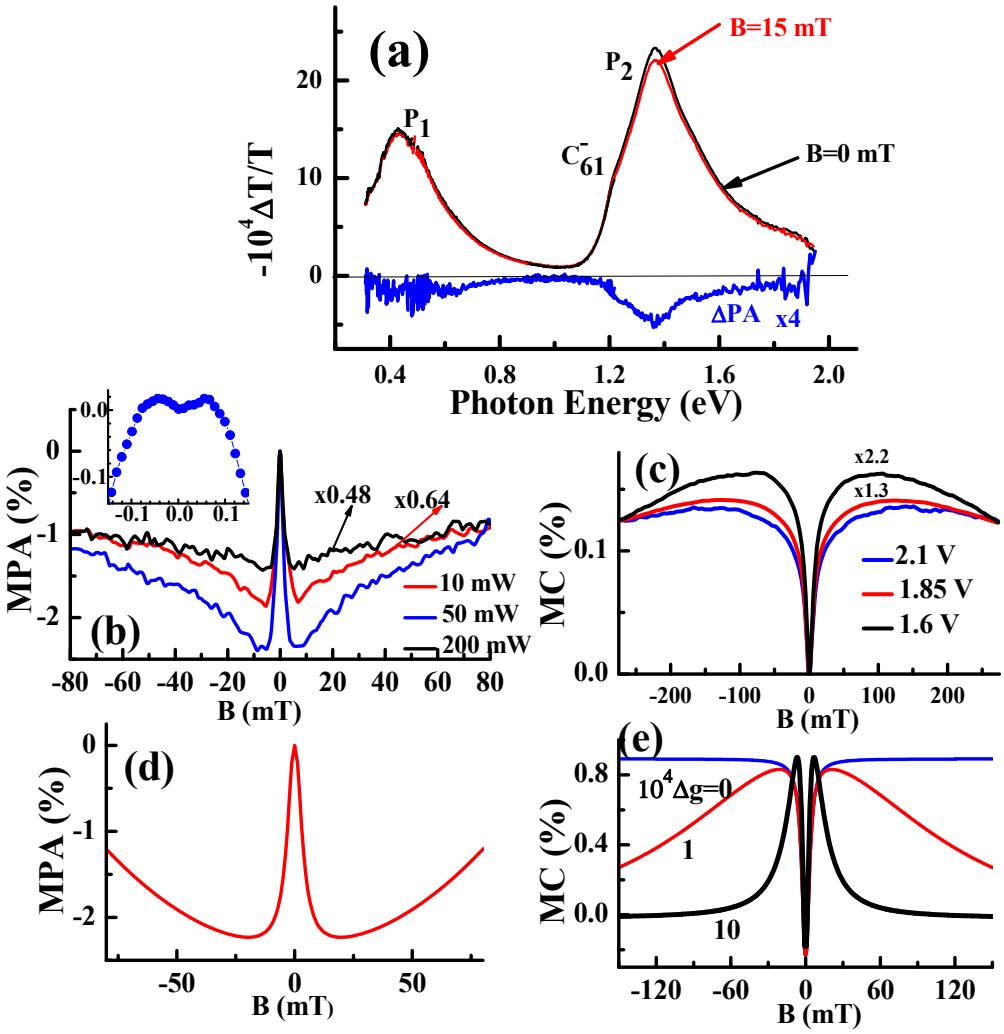
(a)
B=15 mT
P2
P1
C61-
B=0 mT
ΔPA x4
-10^4ΔT/T
Photon Energy (eV)
(b)
x0.48
x0.64
10 mW
50 mW
200 mW
MPA (%)
B (mT)
(c)
x2.2
x1.3
2.1 V
1.85 V
1.6 V
MC (%)
B (mT)
(d)
MPA (%)
B (mT)
(e)
10^4Δg=0
1
10
MC (%)
B (mT)

Figure 4